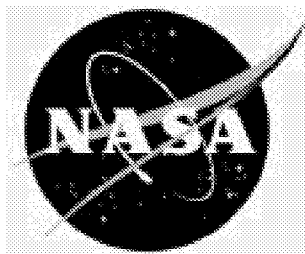# Ultra Narrowband Optical Filters for Water Vapor Differential Absorption Lidar (DIAL) Atmospheric Measurements

Ingrid Stenholm
Lund University, Lund, Sweden

Russell J. DeYoung
Langley Research Center, Hampton, Virginia

December 2001

The NASA STI Program Office . . . in Profile

Since its founding, NASA has been dedicated to the advancement of aeronautics and space science. The NASA Scientific and Technical Information (STI) Program Office plays a key part in helping NASA maintain this important role.

The NASA STI Program Office is operated by Langley Research Center, the lead center for NASA's scientific and technical information. The NASA STI Program Office provides access to the NASA STI Database, the largest collection of aeronautical and space science STI in the world. The Program Office is also NASA's institutional mechanism for disseminating the results of its research and development activities. These results are published by NASA in the NASA STI Report Series, which includes the following report types:
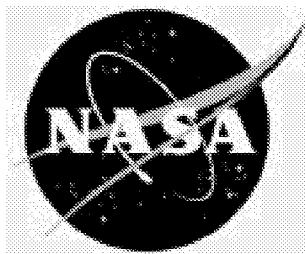
- TECHNICAL PUBLICATION. Reports of completed research or a major significant phase of research that present the results of NASA programs and include extensive data or theoretical analysis. Includes compilations of significant scientific and technical data and information deemed to be of continuing reference value. NASA counterpart of peer-reviewed formal professional papers, but having less stringent limitations on manuscript length and extent of graphic presentations.

- TECHNICAL MEMORANDUM. Scientific and technical findings that are preliminary or of specialized interest, e.g., quick release reports, working papers, and bibliographies that contain minimal annotation. Does not contain extensive analysis.

- CONTRACTOR REPORT. Scientific and technical findings by NASA-sponsored contractors and grantees.

- CONFERENCE PUBLICATION. Collected papers from scientific and technical conferences, symposia, seminars, or other meetings sponsored or co-sponsored by NASA.

- SPECIAL PUBLICATION. Scientific, technical, or historical information from NASA programs, projects, and missions, often concerned with subjects having substantial public interest.

- TECHNICAL TRANSLATION. English-language translations of foreign scientific and technical material pertinent to NASA's mission.

Specialized services that complement the STI Program Office's diverse offerings include creating custom thesauri, building customized databases, organizing and publishing research results . . . even providing videos.

For more information about the NASA STI Program Office, see the following:

- Access the NASA STI Program Home Page at *http://www.sti.nasa.gov*

- Email your question via the Internet to help@sti.nasa.gov

- Fax your question to the NASA STI Help Desk at (301) 621-0134

- Telephone the NASA STI Help Desk at (301) 621-0390

- Write to:
  NASA STI Help Desk
  NASA Center for AeroSpace Information
  7121 Standard Drive
  Hanover, MD 21076-1320

Ultra Narrowband Optical Filters for Water Vapor Differential Absorption Lidar (DIAL) Atmospheric Measurements

Ingrid Stenholm
Lund University, Lund, Sweden

Russell J. DeYoung
Langley Research Center, Hampton, Virginia

December 2001

Contents

Symbols

$A(z)$, $B(z)$	Z-dependent amplitudes of two modes
B	static magnetic flux, gauss
CART	cloud and radiation testbed
CCW	counterclockwise
CW	clockwise
D	diameter of telescope
D_{diff}	minimum diameter of total energy
DIAL	differential absorption lidar
d	distance between atoms
d	length of medium, cm
E_1, E_2	transverse mode patterns
FWHM	full width, half maximum
f	focal length of telescope
K	spatial frequency
k	constant between 1 and 1.5 for wavelengths in visible spectrum
k_0	propagation number
L	length
LASE	Lidar Atmospheric Sensing Experiment
lidar	light detection and ranging
$N(R)$	water vapor concentration between R_1 and R_2
N_b	number of counts/sec from background solar light
N_d	number of counts/sec from detector dark current
N_s	number of counts/sec from water vapor DIAL signal
n	refractive index
n_{eff}	effective refractive index

n_0	original fiber refractive index
R, r	defined by equations (19) and (18), respectively
R_1, R_2	ranges
S/N	signal-to-noise ratio
STP	standard temperature and pressure
S_{off}	lidar signal return amplitude at off-line wavelength
S_{on}	lidar signal return amplitude at on-line wavelength
T	measurement time
V	factor of proportionality (Verdet constant), min of arc/gauss/cm
x, y, z	coordinates
β	propagation constant
β_1	propagation constant of forward progagating mode
β_2	propagation constant of backward propagating mode
Γ	phase mismatch
γ	line width, pm
Δn	amplitude of change in refractive index compared with n_o
$\Delta\lambda$	wavelength separation between laser on- and off-lines
$\Delta\sigma$	differential absorption cross section between on- and off-line wavelengths
κ	coupling coefficient
Λ	spatial period of grating
λ	wavelength
λ_0	wavelength of incident light
σ	cross section
ϕ, θ	polar coordinates

1. Introduction

1.1. Atmospheric Water Vapor

Atmospheric water vapor exists mainly in the troposphere, i.e., the part of the atmosphere that is closest to the Earth, from ground to 10 km. The concentration decreases nearly exponentially with height, as shown in figure 1 (ref. 1), and varies rather smoothly with longitude but decreases rapidly poleward. Even though water vapor only exists in small amounts, it plays a fundamental role in many atmospheric processes such as the atmospheric energy budget, global water cycle, atmospheric chemistry, and transport of pollution.

Climate change is caused by complex interactions among many elements such as radiation, clouds, aerosols, precipitation, atmospheric circulation, and greenhouse gases. Water vapor is the main factor in cloud formation (which impacts precipitation) and in severe storm development. Water vapor is also the most important greenhouse gas and is responsible for maintaining the current climate in that it absorbs the longwave reradiation from the surface of the Earth.

The surface temperature of the Earth depends on the absorbed solar radiation and the rate at which energy is reradiated from the surface of the Earth to space. The rate of reradiation in the atmosphere depends on the amount and the vertical distribution of clouds, aerosols, and greenhouse gases, especially water vapor. It acts as a buffer for the rise and fall of temperature. When the temperature drops to the dew point, water vapor condenses, releasing heat, and the temperature rises again. On the other hand when the temperature rises, water vapor evaporates, taking up heat, and in this way cooling the atmosphere.

Most climate models show that an initial warming of the climate results in a significant increase in water vapor that then amplifies the initial warming. Therefore an increase in other greenhouse gases,
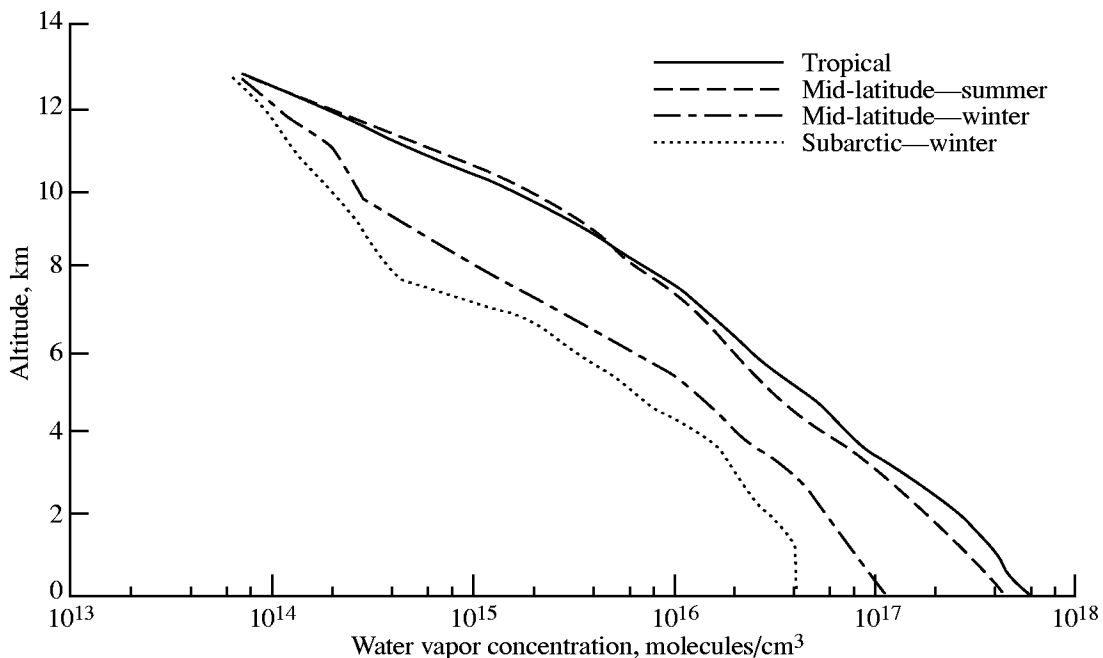

Figure 1. Water vapor concentration profiles for indicated latitudinal bands and seasons. (See ref. 1.)

such as CO_2, causes a warming of the climate that causes an increase in atmospheric water vapor, which results in further warming when the water vapor absorbs reradiation from the Earth to the sky. The saturation vapor pressure increases exponentially with temperature; therefore, the abundance of water vapor can provide a very important increase in atmospheric temperature.

The latent heat of water vapor also channels energy into the atmosphere, and it is the main energy source for hurricane development. Understanding the distribution of water vapor around a hurricane may one day allow the prediction of hurricane intensity and direction.

A better understanding of the horizontal and vertical distribution and transport of water vapor is essential for understanding the processes that regulate climate and to better predict future climate changes and their regional and global impacts. The use of lidar onboard NASA research aircraft has allowed the measurement of the atmospheric water vapor distribution during different campaigns around the world. In the future, lidar systems will be deployed on Earth-orbiting satellites to measure the global water vapor distribution (refs. 2, 3, and 4).

1.2. Lidar Measurement of Water Vapor

Lidar (light detection and ranging) is a method that has been used since the 1960's to detect particles or gases in the atmosphere. A laser is used to send out short pulses of light. The pulse travels with the speed of light, 3×10^8 m/s. Some of the radiation is reflected by the atmospheric molecules and aerosols and this back-reflected radiation is collected by a telescope. The distance traveled by the light to a point in the atmosphere is equal to the speed of light times half the round-trip travel time from the laser transmitter to the receiver. The radiation is analyzed, and the density of the atmosphere is then determined. Where the density is higher, a stronger backscattered signal is received. The atmospheric density is higher closer to the Earth; therefore, the return signal decreases with increasing distance from the Earth.

Lidar is an active remote sensing method, which means that light is sent out actively as a laser pulse instead of using light from the Sun. This method gives more freedom because the system is not dependent on sunlight. There are several different ways of using a lidar system. It is easy to mount it on a truck, an airplane, or even a satellite so that the measurements can be made at many different places. A lidar system in orbit around the Earth has many advantages, such as high resolution and complete Earth coverage.

Lidar uses a single wavelength that scatters off atmospheric molecules and aerosols but cannot distinguish between different atmospheric species. There are two main kinds of scattering, Rayleigh and Mie. Rayleigh scattering, also called molecular scattering, is scattering of light by objects that are small in comparison with the laser wavelength. The scattered flux density is inversely proportional to the fourth power of the laser wavelength. Mie scattering, also called aerosol scattering, is scattering by particles that are larger than the wavelength of the radiation. The scattered flux density is inversely proportional to λ^k, where k is a constant between 1 and 1.5 for wavelengths in the visible spectrum.

To measure the density of an atmospheric species such as water vapor, a more advanced lidar technique is used. This technique is a special development of lidar called differential absorption lidar (DIAL) (ref. 4).

1.3. DIAL Technique

Differential absorption lidar can provide long-range high-resolution measurements of atmospheric H_2O. DIAL is based on the fact that different atoms and molecules absorb different laser wavelengths. In DIAL, two different wavelengths are sent into the atmosphere, one that will be absorbed by the particle of interest such as water vapor and another wavelength that does not experience water vapor absorption. Both wavelengths are near each other so that they experience the same atmospheric molecular scattering. By comparing the decay of the backscattered light from the absorbed wavelength with the decay of the backscattered light from the nonabsorbed wavelength, the concentration of water vapor can be determined as a function of range.

The simplified DIAL equation for determining the average water vapor concentration $N(R)$ between the ranges R_1 and R_2 is given by (ref. 5)

$$N(R) = \frac{1}{2\,\Delta\sigma(R_2 - R_1)}\,\ln\left[\frac{S_{on}(R_1)\,S_{off}(R_2)}{S_{on}(R_2)\,S_{off}(R_1)}\right] \tag{1}$$

where S_{on} and S_{off} are the lidar signal return amplitudes at the on- and off-line wavelengths, respectively. The lidar wavelengths are selected to be on the peak of the water vapor (such as 946.0003 nm) absorption and in an unabsorbed region off the peak (such as 945.9 nm), $\Delta\sigma$ is the differential absorption cross section between the on- and the off-line wavelengths, and $(R_2 - R_1)$ is the range cell over which the average concentration is measured. Equation (1) assumes that the wavelength separation between on and off laser lines is small ($\Delta\lambda \leq 0.1$ nm). In this case, aerosol backscatter and atmospheric extinction errors are negligible, and the laser lines are selected so that there is negligible interference from other atmospheric gases.

Figure 2 shows the concentration of water vapor in the troposphere measured with different methods (private communication from Syed Ismail et al., Langley Research Center). The solid curve is a Lidar Atmospheric Sensing Experiment (LASE) measurement which uses the DIAL technique. As the figure shows the DIAL measurement corresponds very well to the other methods such as Raman lidar and balloon sondes.

In the future, a DIAL laser system will be placed on a satellite in space to continuously measure the atmospheric water vapor. Such a system would make it possible to predict the weather a month in advance by measuring the global distribution of water vapor. The water vapor lines of interest for a space-based DIAL system are the 940-nm water vapor band lines as shown in figure 3. These lines are of interest because of their very high absorption cross section (refs. 4, 5, and 6).

1.4. Importance of Narrowband Receiver Filters in DIAL System

In an Earth-orbiting satellite optical detection system, some of the sunlight that is reflected by the surface of the Earth and the atmosphere will always enter the telescope as noise. By reducing the optical bandwidth of the receiver, the noise is also reduced. To make good measurements, the signal must be larger than the noise or the signal-to-noise ratio should be greater than 1.

The signal-to-noise ratio for a photon counting receiver system is given by (ref. 5)

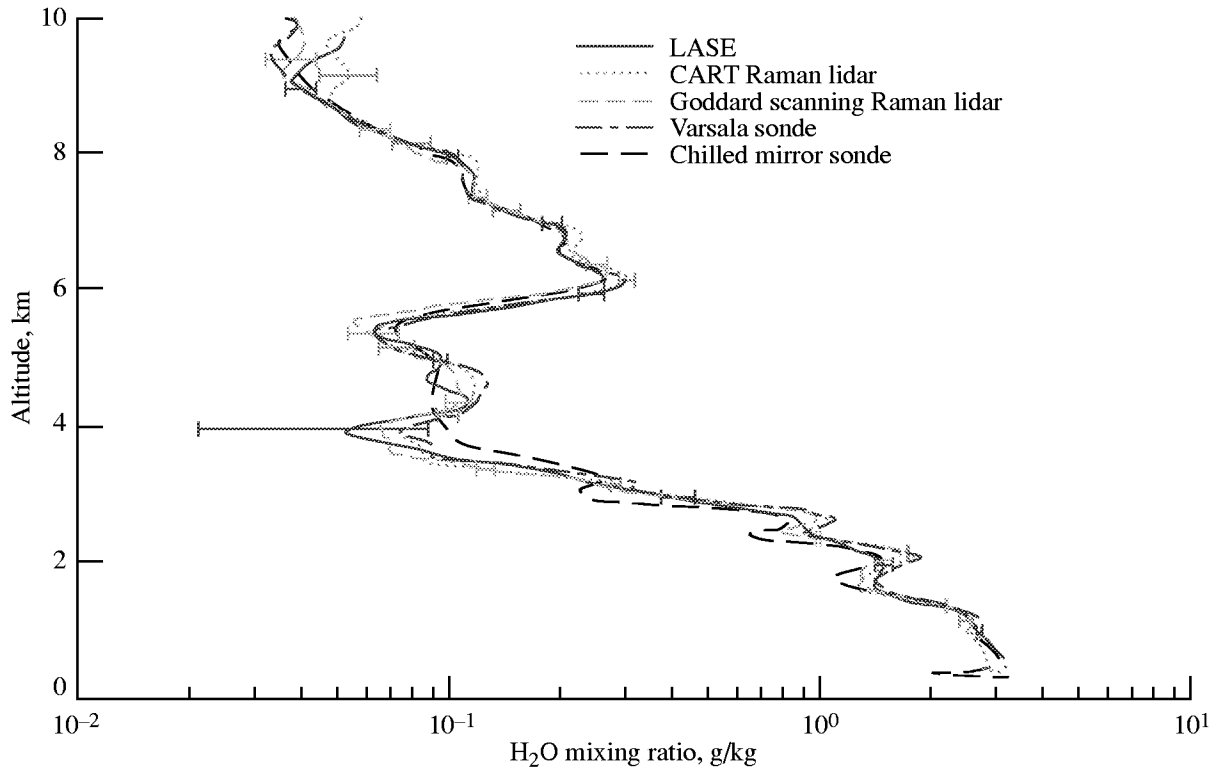$$\frac{S}{N} = \frac{N_s\sqrt{T}}{\sqrt{N_s + 2(N_b + N_d)}} \tag{2}$$

3

Figure 2. Concentration of atmospheric water vapor (grams of water vapor per kilograms of air) in the troposphere.

A $\lambda = 945.4075$
   $\sigma = 0.709 \times 10^{-22}$ cm^2
   $\gamma = 7.29$ pm STP

B $\lambda = 945.4658$
   $\sigma = 0.75 \times 10^{-22}$ cm^2
   $\gamma = 8.26$ pm

C $\lambda = 945.6151$
   $\sigma = 1.96 \times 10^{-22}$ cm^2
   $\gamma = 4.88$ pm

   $\lambda = 945.6208$
   $\sigma = 0.714 \times 10^{-22}$ cm^2
   $\gamma = 4.88$ pm

D $\lambda = 946.0003$
   $\sigma = 2.89 \times 10^{-22}$ cm^2
   $\gamma = 8.47$ pm

E $\lambda = 946.1240$
   $\sigma = 0.845 \times 10^{-22}$ cm^2
   $\gamma = 5.52$ pm

   $\lambda = 946.1356$
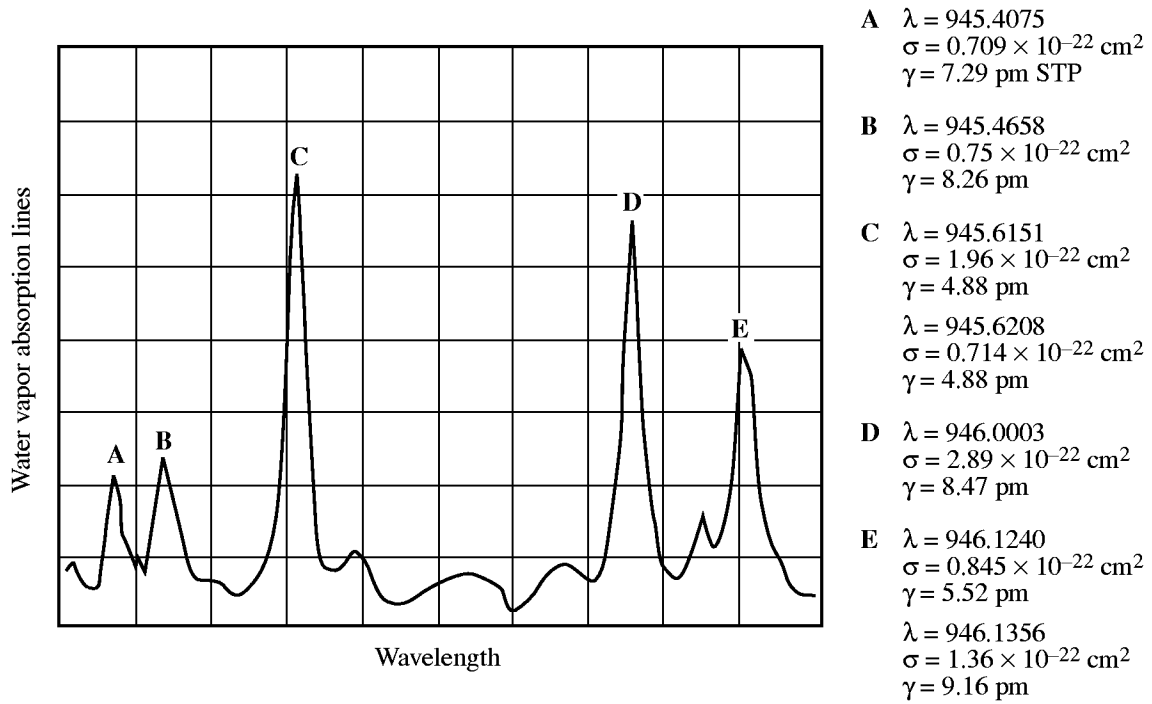 $\sigma = 1.36 \times 10^{-22}$ cm^2
   $\gamma = 9.16$ pm

Figure 3. Water vapor absorption spectrum showing water vapor absolute lines λ, corresponding absorption cross sections σ, and FWHM line widths γ.

4

To improve S/N, the signal return N_s could be made larger by building a higher energy laser on the satellite, which is a very expensive option. If the measurement time T is increased, S/N increases but the horizontal resolution of the water vapor measurement decreases. To get good measurements, a compromise has to be made between S/N and the horizontal resolution. The background noise signal N_b and the detector noise N_d should be as small as possible; N_d depends on the detector chosen and to make it small a very good low-noise detector is needed; N_b should also be as small as possible. To do this, an optical filter is placed in front of the detector. The filters used today are typically 300-pm FWHM but this could be reduced with fiber Bragg grating filters to 20 pm FWHM. Figure 4 shows a future space-based water vapor DIAL system. Figure 5 (private communication from Syed Ismail, Langley Research Center, and Susan Kooi, SAIC) shows a simulation of such a system orbiting at an altitude of 400 km using a 500-mJ laser energy at 10 Hz (940 nm) with a 1-m-diameter receiver telescope having a detector quantum efficiency of 40 percent. The horizontal water vapor resolution is 100 km and the vertical resolution is 1 km. Using different cross sections at different heights is necessary because the water vapor concentration decreases a lot with increasing distance from Earth. The difference in the two sets of graphs is the filter bandwidth, either 300 or 20 pm FWHM. The daytime operation filter transmission is 30 percent for the 20-pm filter and is 50 percent for the 300-pm filter. Cross sections are given in units of $\times~10^{-24}$ cm^2. When using a 20-pm filter instead of a 300-pm filter, the random error decreases by about a factor of 2 from altitudes of 5 to 10 km.

1.5. Research Objectives

The primary goal of this research effort is to demonstrate and characterize the performance of an ultra narrowband optical fiber Bragg grating filter at 940 nm, which corresponds to the water vapor lines of interest for space-based DIAL measurements. A tunable diode laser is used to determine the bandwidth and efficiency of the filter and then these measurements are compared with theoretical calculations. Laser radiation enters a 30-cm-diameter Newtonian telescope, where an optical fiber is placed at the focal point. Once the radiation is in the fiber, it is transmitted to a reflective fiber Bragg grating which acts as an optical filter. The efficiencies of each leg of this filter concept are measured so that overall filter performance can be determined. Suggestions for improvements in performance are then stated.

2. Theory of Fiber Bragg Gratings

2.1. Bragg Gratings

Fiber Bragg gratings are based on the development of diffraction gratings. A grating is made up of a periodic reflective surface or structure. When light falls onto the grating, wavelengths whose traveling
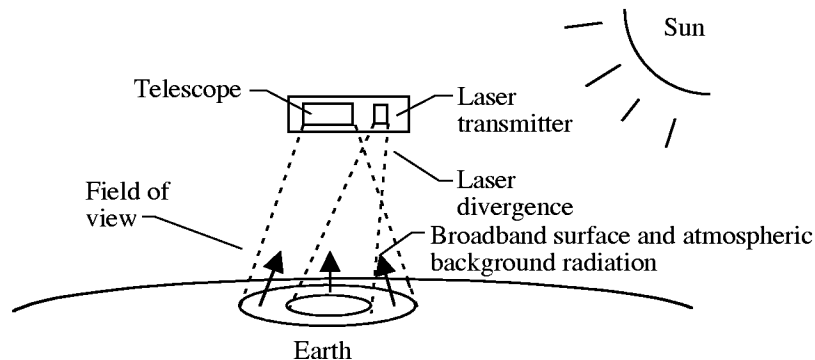

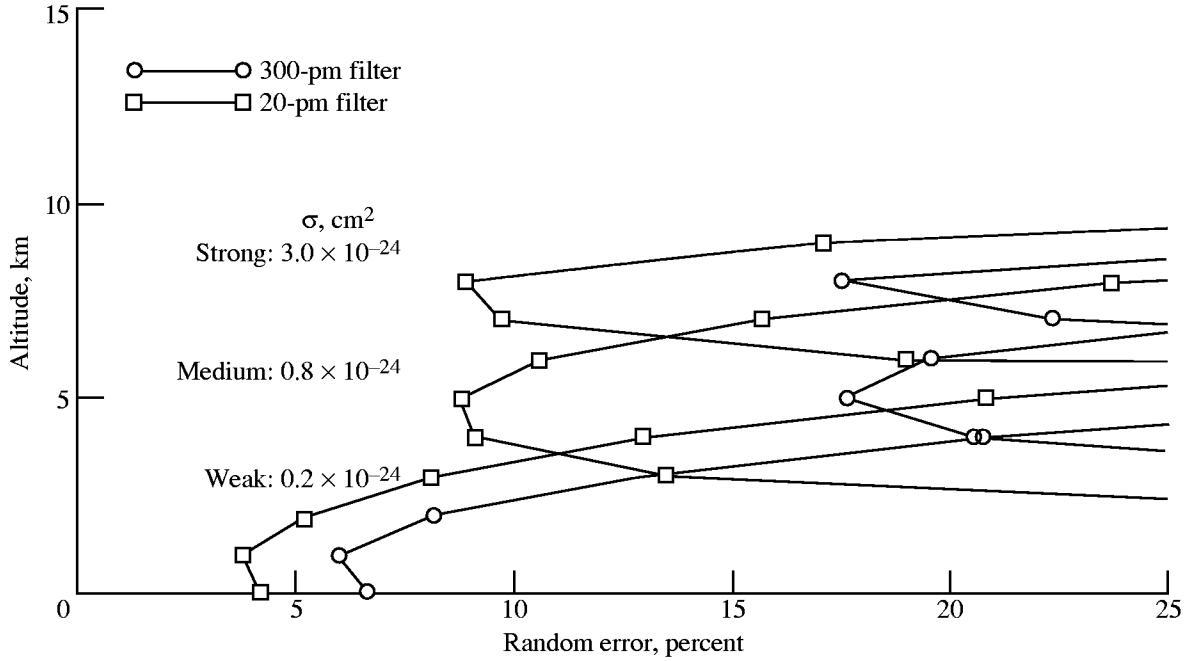Figure 4. Space-based water vapor DIAL system.

Figure 5. Modelling of error in water vapor atmospheric profile measured from space-based satellite for three different water vapor absorption cross sections with either 50-percent transmission, 300-pm FWHM filter or 30-percent transmission, 20-pm FWHM filter.
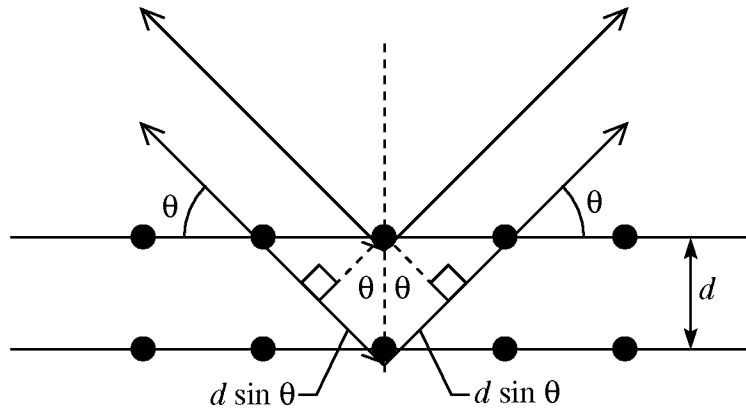

Figure 6. Bragg reflection from a periodic group of atoms.

distance corresponds to an integer times the wavelength will constructively interfere making an interference maximum as shown in figure 6.

Radiation is incident on a crystal, where the distance between the atoms is d. The ray that is reflected from the lower layer of atoms must travel a distance $2d \sin \theta$ farther than the upper ray. For the reflected rays to reinforce each other, this extra path length must be an integer multiple of λ, which is exactly what Bragg's law tells us:

$$n\lambda = 2d \sin \theta \qquad (n = 1,2,3,...) \tag{3}$$

2.2. Fiber Bragg Gratings

If a germanium-doped silica core fiber is exposed to ultraviolet radiation there will be a permanent change in the core refractive index. A periodic refractive index change (i.e., a grating) in a fiber is accomplished by exposing the germanium-doped silica core fiber to periodic ultraviolet laser light. Interfering laser beams are used to produce a mask that is then applied to the germanium-doped fiber resulting in refractive index changes where the beams interfere constructively and there is no change in the regions of destructive interference. The degree of index change depends on the amount of time the UV laser source is applied to the fiber. Thus very precise periodic index changes can be created in the fiber.

When light propagates through a fiber where a grating has been induced and if the Bragg condition is satisfied, the forward propagating light will be strongly coupled to the grating, which results in light propagating in the backwards direction. To satisfy the Bragg condition, the difference in the propagation constants of the two coupled modes must be equal to the spatial frequency K as

$$\beta_1 - (-\beta_2) = K = \frac{2\pi}{\Lambda} \tag{4}$$

where β_1 and β_2 are the propagation constants of the forward propagating mode and the backward propagating mode, respectively, and Λ is the spatial period of the grating as shown in figure 7. The case of contradirectional coupling describes coupling when two modes with the same propagation constant are traveling in opposite directions.

For contradirectional mode coupling, the total electric field can be described by

$$E(x,z) = A(z)\, E_1(x)\, e^{-i\beta_1 z} + B(z)\, E_2(x)\, e^{i\beta_2 z} \tag{5}$$
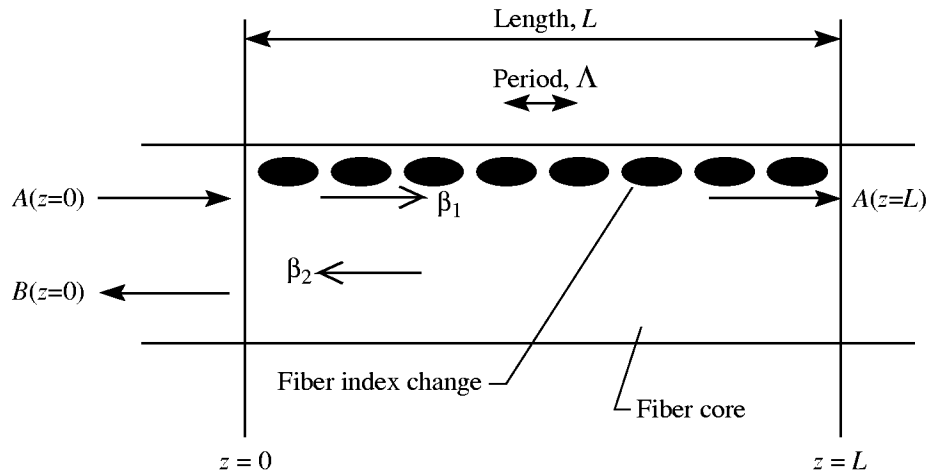
Figure 7. Fiber grating and incoming and reflected beam modes.

7

By inserting equation (5) into the wave equation for modes in a fiber in the absence of any perturbation and solving these equations give the following two equations that describe how the amplitudes vary with z:

$$\frac{dA}{dz} = \kappa B \, e^{i\Gamma z} \tag{6a}$$

$$\frac{dB}{dz} = \kappa A \, e^{-i\Gamma z} \tag{6b}$$

where κ is the coupling coefficient describing the coupling between the modes in the fiber and is therefore dependent on the index, wavelength of operation, and the extent of the periodic perturbation; Γ is the phase mismatch given by the difference in propagation constants, β_1 and β_2, with the spatial frequency K subtracted; thus

$$\Gamma = \beta_1 - (-\beta_2) - K \tag{7}$$

In our case, we require phase matching, implying $\Gamma = 0$ or

$$\beta_1 + \beta_2 = K \tag{8}$$

Since the two modes are identical, the propagation constants are the same; thus

$$\beta_1 = \beta_2 = \frac{2\pi}{\lambda_0} n_{\text{eff}} \tag{9}$$

where n_{eff} is the effective index of the mode, that is, the actual refractive index under these conditions, and

$$n_{\text{eff}} = \frac{\beta_1}{k_0} = \frac{\beta_2}{k_0} \tag{10}$$

where k_0, the propagation number, is

$$k_0 = \frac{2\pi}{\lambda_0} \tag{11}$$

and λ_0 is the wavelength of the incident light. The spatial frequency K was defined in equation (4) as

$$K = \frac{2\pi}{\Lambda} \tag{12}$$

where Λ is the period of the grating. Equations (8) and (9) are used to get the following final expression of the period of the grating at the wavelength of operation (ref. 7):

$$\Lambda = \frac{\lambda_0}{2n_{\text{eff}}} \tag{13}$$

2.3. Derivation of Grating Reflectivity

Equation (6b) is differentiated with respect to z and using equation (6a) we obtain

$$\frac{d^2 B}{dz^2} = \kappa^2 B \tag{14}$$

When solving this equation and substituting the solution into equation (6b), the following equations are obtained:

$$B(z) = b_1 e^{\kappa z} + b_2 e^{-\kappa z} \tag{15a}$$

$$A(z) = b_1 e^{\kappa z} - b_2 e^{-\kappa z} \tag{15b}$$

If we assume unit power incident in mode A on a periodic waveguide of length L, $A(z=0) = 1$. There is no back-coupled wave beyond $z = L$; thus, $B(z=L) = 0$. Solving equations (15) with these boundary conditions, the following two expressions are obtained:

$$b_1 = \frac{e^{-\kappa L}}{2 \cosh \kappa L} \tag{16a}$$

$$b_2 = \frac{-e^{\kappa L}}{2 \cosh \kappa L} \tag{16b}$$

Thus, the equations describing the amplitudes of the modes are

$$B(z) = \frac{\sinh \kappa(z - L)}{\cosh \kappa L} \tag{17a}$$

$$A(z) = \frac{\cosh \kappa(z - L)}{\cosh \kappa L} \tag{17b}$$

where $B(z)$ is the reflected mode; therefore, we can define a reflection coefficient as

$$r = \frac{B(z=0)}{A(z=0)} = -\tanh \kappa L \tag{18}$$

The energy reflection coefficient is then

$$R = |r|^2 = \tanh^2 \kappa L \tag{19}$$

9

A medium of refractive index n with a periodic refractive index grating given by

$$n(z) = n_0 + \Delta n \ \sin\frac{2\pi}{\Lambda} z \tag{20}$$

has a coupling coefficient of

$$\kappa = \frac{\pi \ \Delta n}{\lambda_0} \tag{21}$$

Substituting equation (21) into (19) gives the final expression for the reflectivity of a fiber grating of length L as (ref. 7)

$$R = \tanh^2\left(\frac{\pi \ \Delta n \ L}{\lambda_0}\right) \tag{22}$$

Figure 8 shows the grating reflectivity plotted from equation (22). As the length of the grating increases, the grating approaches 100 percent reflectivity for a given Δn. Also when the amplitude of the periodic refractive index change Δn increases, the reflectivity also increases. To get a grating with high reflectivity and narrow bandwidth, a compromise is necessary between the high Δn needed to get high reflectivity and the lower Δn needed to get a narrow bandwidth. The stars in the figure correspond to values measured in the laboratory and are discussed later.
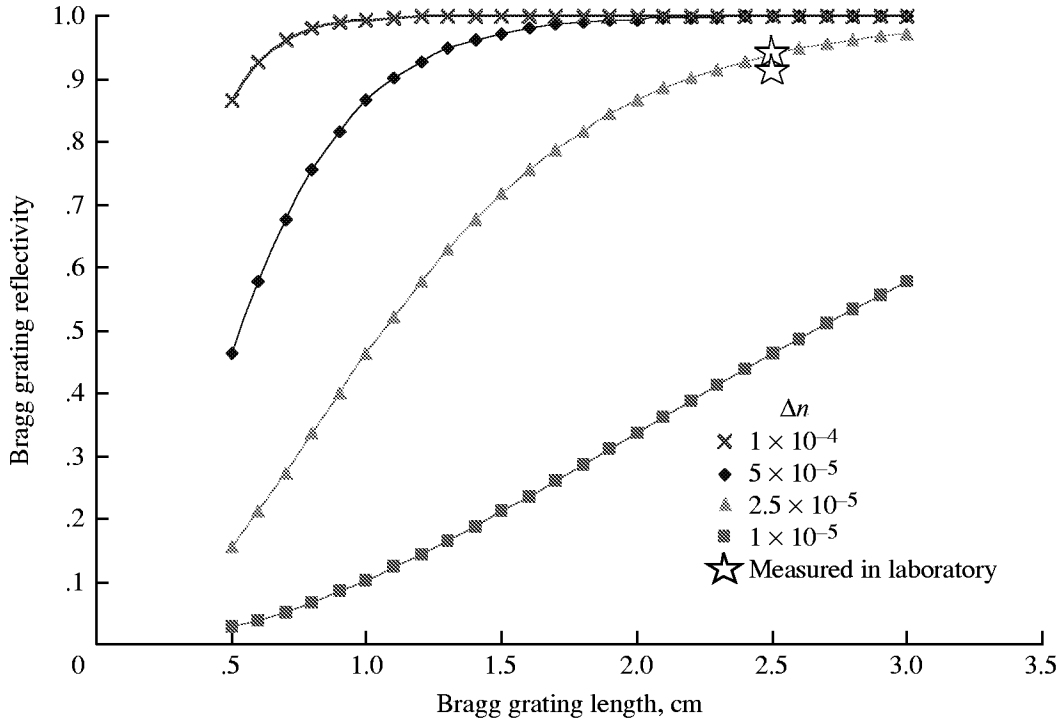

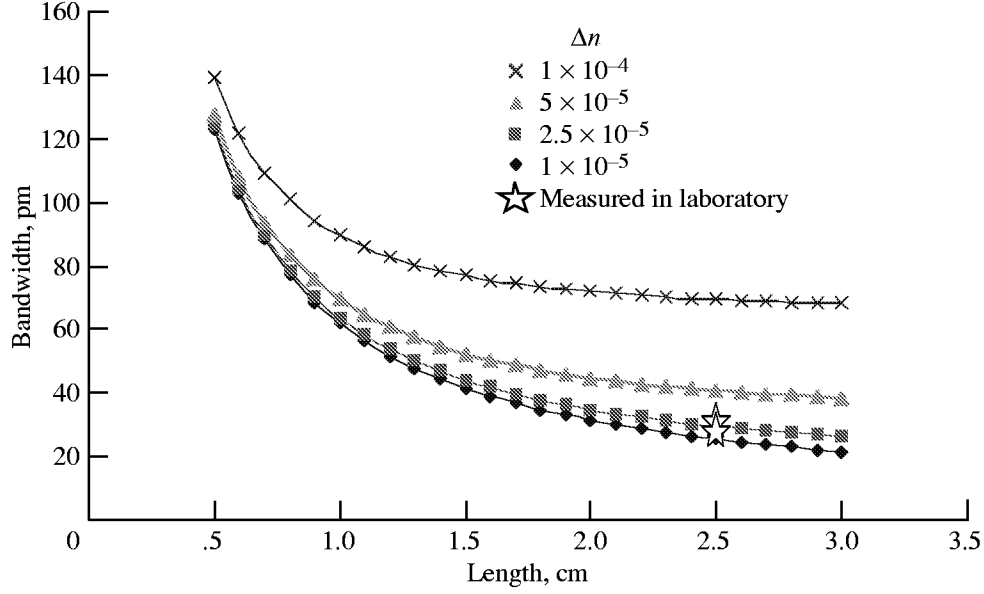Figure 8. Bragg grating reflectivity versus grating length at 946 nm.

Figure 9. Bragg grating bandwidth versus grating length at wavelength 946 nm.

2.4. Bragg Grating Bandwidth Expression

By solving the equation for the reflection coefficient (eq. (19)) for the first minimum at one side of the reflectivity peak and multiplying it by 2 to get the whole bandwidth, from minimum to minimum, we get the corresponding bandwidth of the fiber Bragg grating as (refs. 7 and 8)

$$\Delta\lambda_0 = \frac{\lambda_B^2}{\pi n_{eff} L}(\kappa^2 L^2 + \pi^2)^{1/2} \tag{23}$$

where $\lambda_B = \lambda_0$ is the wavelength that is reflected by the fiber grating.

Figure 9 shows a plot of the Bragg grating bandwidth in pm from equation (23) versus the length of the grating. The wavelength used is 946 nm, which is also the wavelength that was used in the experiments. It shows that the bandwidth decreases when the length of the grating is increased. The bandwidth of the grating also decreases when Δn, the amount of the periodic refractive index change, decreases. The stars represent the values that have been measured in the laboratory and are discussed later.

3. Experimental setup

3.1. Typical Water Vapor DIAL Receiver Setup

Figure 10 shows a general picture of how the fiber Bragg receiver would be used in a typical space DIAL application for the measurement of water vapor at 946 nm. The Newtonian telescope collects some of the light that has been backscattered by the particles in the atmosphere. This light is focused onto a single mode fiber that is connected to an optical circulator where light travels from port 1 to port 2. Attached to port 2 are fiber Bragg gratings which reflect light at a specific wavelength. The DIAL on- and off-line wavelengths at 946.0003 nm and 945.9 nm are reflected by the fiber Bragg gratings, enter the circulator again at port 2, and leave at port 3, where this light is detected by an avalanche
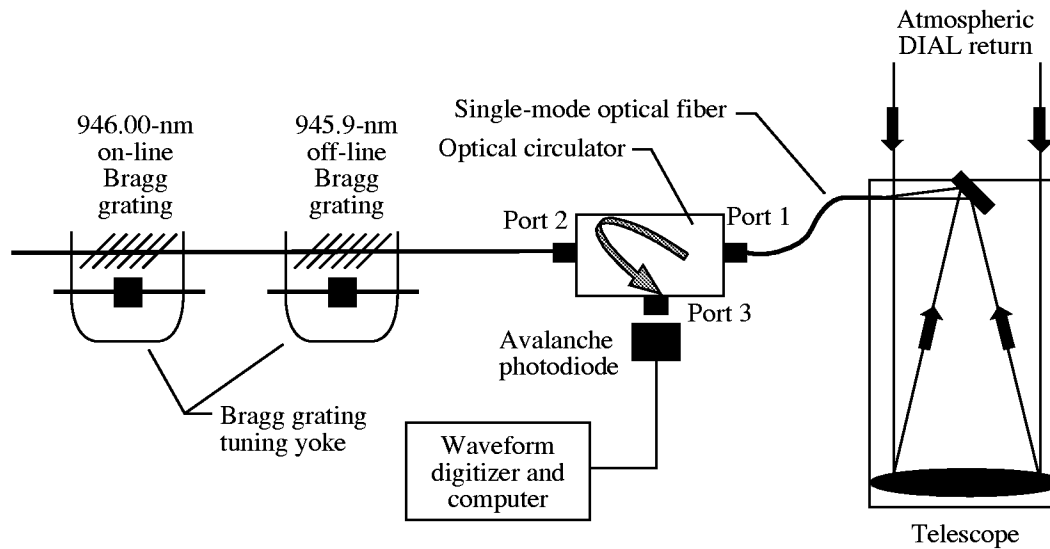
Figure 10. Fiber Bragg filter receiver concept for typical space-based DIAL application.

photodiode. The signal from the detector is digitized and sent to a computer for storage and processing. The yokes are used to tune the fiber reflection wavelength. By stretching the fiber, the period of the grating is increased, and according to equation (13), a higher wavelength is reflected.

3.2. Laboratory Experimental Setup

To determine the optical bandwidth and efficiency of this receiver concept, the setup shown in figure 11 was constructed. The laser used was an external-cavity tunable diode laser from New Focus Inc., Model 6238, which could be tuned from 930 to 966 nm, with a maximum power output of 30 mW and line width of 0.014 pm at 940 nm. The photodiodes are Thorlab DET210 high-speed photodetectors. The absorption cell (Infrared Analysis model number G-4-10-PA) is a 20-m cell, which means that light is multiply reflected 20-m inside the cell. The optical circulator was made by Optics for Research, Inc., model number OC-3-FFT-946-X-Z. The fiber Bragg gratings made by Communication Research Centre Canada, have an on-line wavelength of 946.0 nm and an off-line one of 945.9 nm. The fiber used in the gratings is a single-mode Corning 1060 photonic fiber with a core diameter of 6 μm. The yokes are used to change the wavelength to be reflected by the grating.

The output of the laser is split into two beams. One beam is detected by a photodiode that is connected to the oscilloscope and is used to monitor the output stability of the laser. The other beam is split once again, one beam goes into the water vapor absorption cell, while the other beam goes through the optical circulator unattenuated and enters the fiber at port 2 where fiber Bragg gratings are attached. The on- and off-line wavelengths are reflected by the fiber grating and they reenter the optical circulator and are then directed to port 3 where light is detected by a photodiode. The signal is connected to the oscilloscope to monitor the two reflection peaks from the fiber grating.

3.3. Optical Circulator Description

The optical circulator works in two different ways depending on whether the light enters port 1 or port 2. Either unpolarized or polarized light from the receiver telescope enters fiber port 1 as shown in figure 12. The calcite crystal is a double refractive crystal, which means that it splits the beam into two beams that are orthogonally polarized. The rays that are polarized perpendicular to the optic axis (the
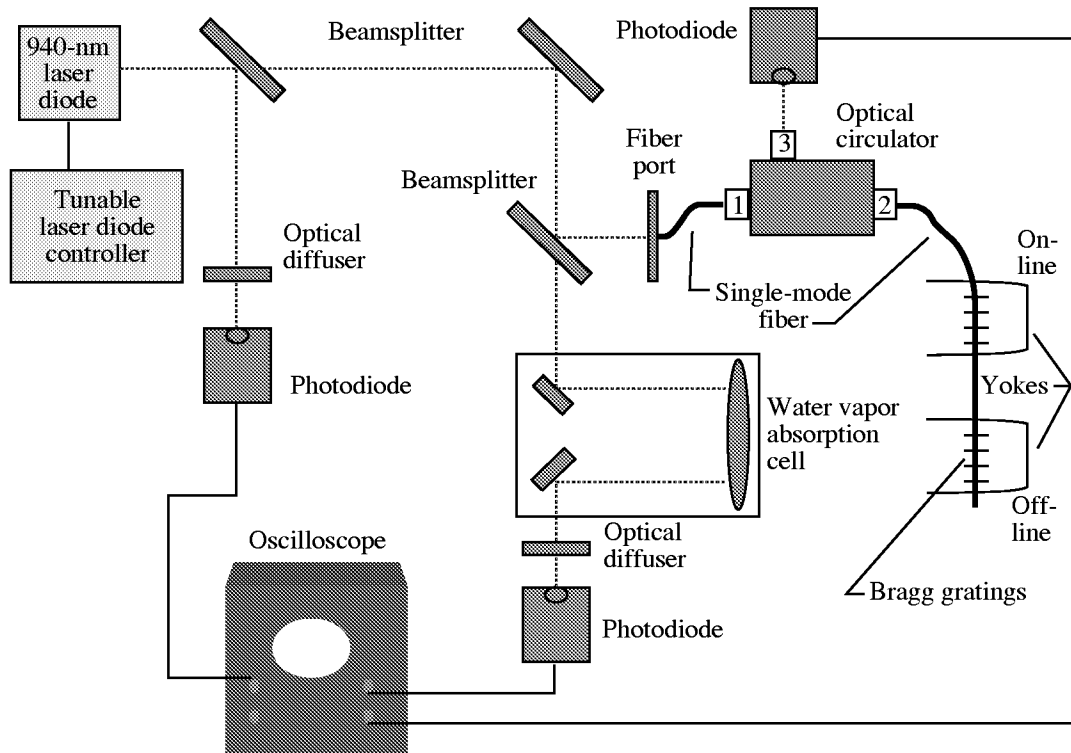
Figure 11. Bragg grating filter measurement setup.
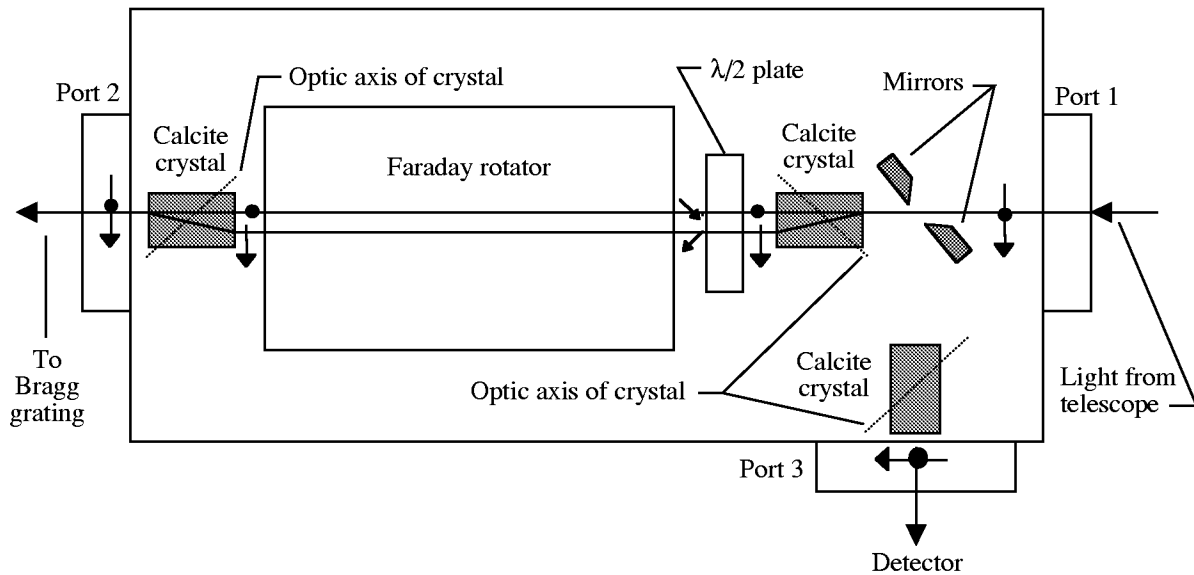
Figure 12. Operation of circulator with input light from telescope.

ordinary rays) pass through the crystal unaffected, but the rays polarized in the plane of incidence (the extraordinary rays) are shifted horizontally as shown. Light comes out of the crystal in two separate beams that are orthogonally polarized. The half-wave (see the appendix) plate rotates the polarization of the beams by 45° having a fast and a slow axis. The slow axis is inclined 22.5° to the horizontal and the fast axis is perpendicular to the slow axis. The half-wave plate rotates the component of the beam that is

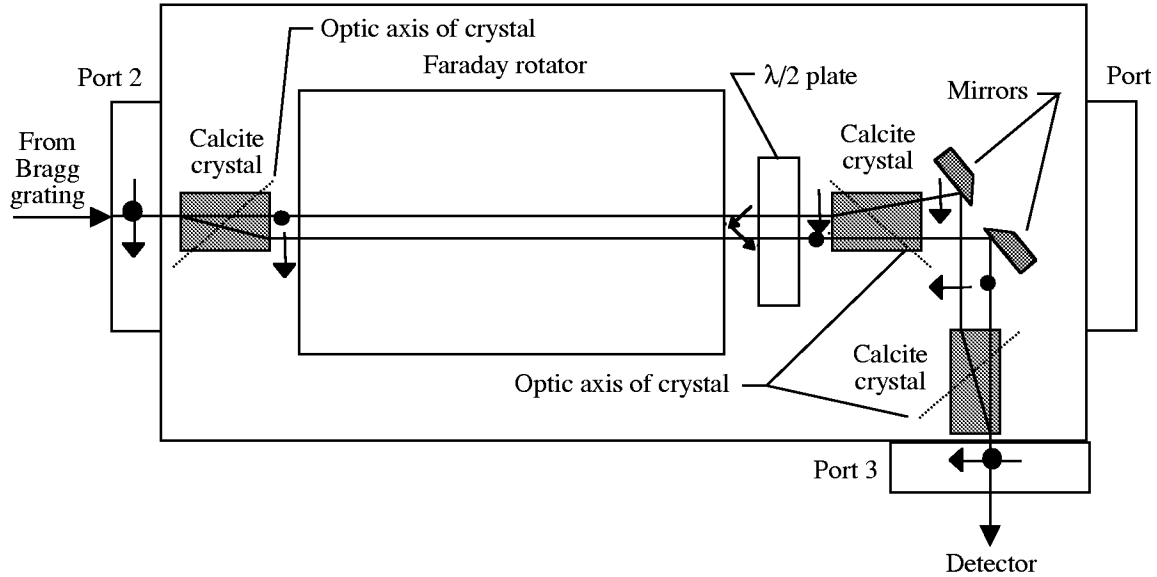Figure 13. Input from fiber Bragg grating at port 2.

polarized parallel to the slow axis by 180°; thus, the total polarization of each beam is rotated 45°. The Faraday rotator (see the appendix) rotates the polarization of the light back 45° so that when light leaves the Faraday rotator it is polarized the same way as before entering the half-wave plate. A Faraday rotator always rotates the polarization of light in the same absolute direction no matter from which direction light enters the rotator. The calcite crystal at port 2 has the optic axis inclined at the same angle as the first crystal but in the opposite direction, which makes the two beams recombine into one beam. Light out of fiber port 2 is now coupled to a single-mode fiber which contains the fiber Bragg gratings.

Light that is reflected by the fiber Bragg gratings enters again at port 2 as shown in figure 13, where the beam is split into two beams, o-beam and e-beam, which are perpendicularly polarized. The Faraday rotator rotates each beam 45°, rotating the polarization in the same absolute direction independent of the direction of propagation. The half-wave plate rotates the polarization 45° more. The Faraday rotator and the half-wave plate have rotated the polarization of the beams a total of 90°. The beam that was the o-beam (vertically polarized) in the first crystal is now the e-beam (polarized in the plane of incidence) and vice versa because of the total rotation of 90°. The e-beam is now shifted in the calcite crystal. Both the e-beam and the o-beam are reflected by the mirrors into the calcite crystal at port 3, which recombines the two beams into one beam. The unpolarized light that comes out of port 3 is detected by a photodiode detector.

3.4. Telescope

To find the focal spot size of the Newtonian telescope, the setup shown in figure 14 was constructed. Laser light is coupled into a fiber that is placed at the focal point of a large parabolic mirror. Parallel light reflected by this mirror enters the receiver telescope consisting of a 30-cm-diameter, 60-cm focal-length parabolic aluminum mirror and is focused at the focal point of the telescope. A charged coupled device (CCD) camera (Edmund Industrial Optics L55-702), pixels 537 (H) × 550 (V) and pixel size 7.15 (H) × 5.55 (V) μm, is placed at the focal point of this mirror to determine the focus spot size and is connected to an oscilloscope and also to a beam profiler which allows the beam spot size
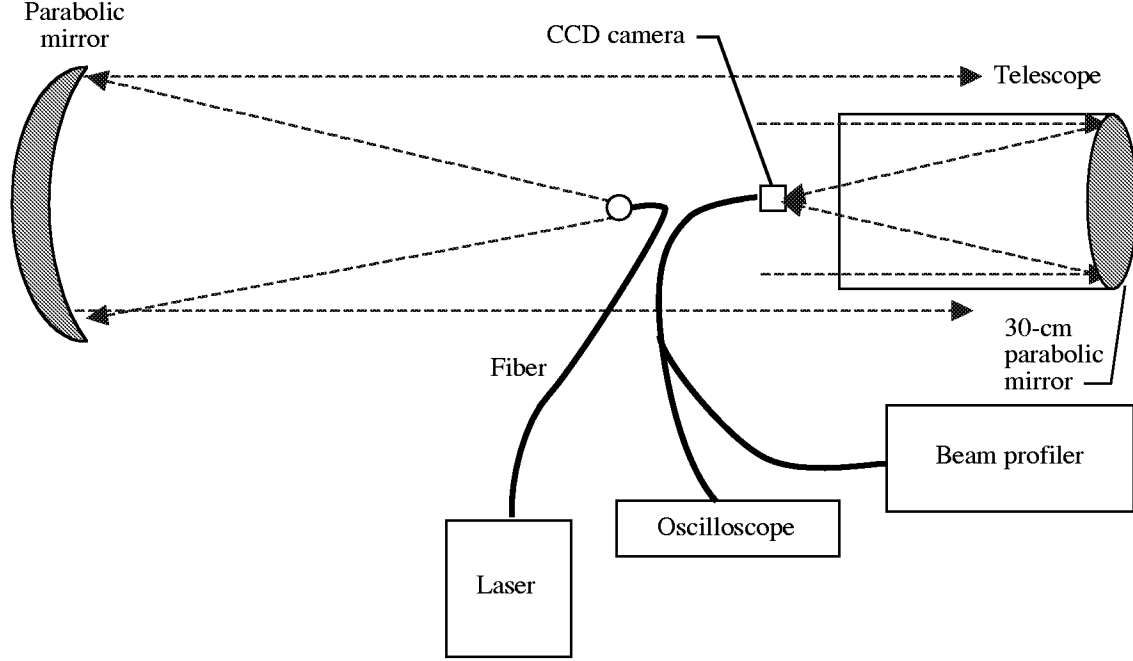
Figure 14. Setup for measuring receiver telescope focus spot size.

to be viewed as measured. The focal spot size is limited by diffraction and theoretically the minimum diameter for 91 percent of total energy D_{diff} is given by

$$D_{\text{diff}} = 4.4\lambda\frac{f}{D} \qquad (24)$$

where f is the focal length of the telescope (60 cm), D is the diameter of the telescope (30 cm), and λ is the wavelength of the light (946 nm) which gives a minimum spot diameter of 8.3 μm. This focal spot size is close to the single-mode fiber to be used to couple the light into the optical circulator.

4. Experimental Results

4.1. Tuning of Fiber Bragg Grating

When the fiber Bragg gratings were received from Communication Research Centre Canada, the bandwidth and wavelength of peak reflectivity were not known because the company did not have the means to measure these gratings. The first research step was to measure the wavelength of the peak reflectivity as well as the FWHM bandwidth. The setup shown in figure 10 was used to identify the reflection wavelengths of the fiber Bragg gratings. The tunable diode laser had its beam split into two beams, one coupled to the fiber Bragg grating using a Optics for Research model PAF-X-5-946 port and the other beam went to a water vapor absorption cell. The output of the cell had a silicon photodiode to measure the water vapor absorption lines. The diode laser was then tuned simultaneously through the fiber Bragg gratings and the water vapor absorption cell. A photodiode at the end of the Bragg grating fiber recorded the absorption and the bandwidth of the two Bragg gratings.

As shown in figure 15, neither of the fiber Bragg gratings overlap water vapor absorption lines. The mask used to make these gratings was slightly off the designed wavelength of 946.0 nm for the on-line
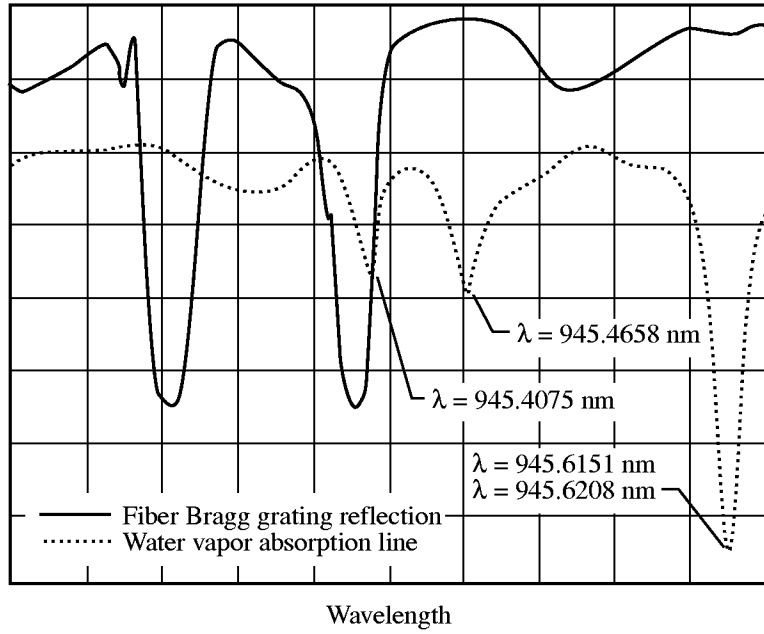
Figure 15. Fiber Bragg grating reflection peaks and water vapor absorption lines.
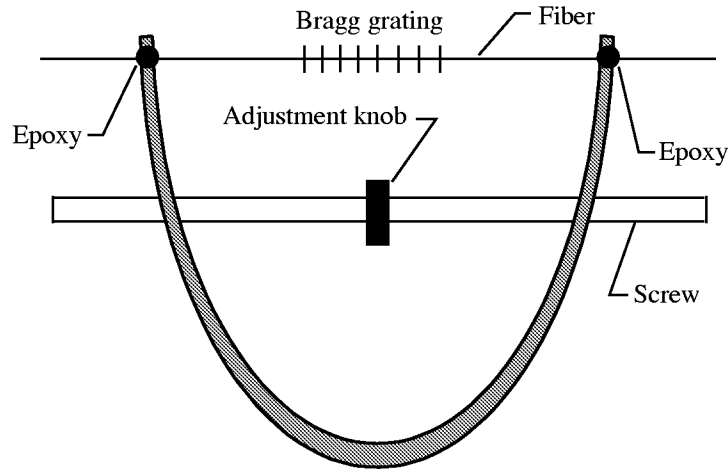
Figure 16. Filter Bragg grating tuning yoke.

grating and 945.9 nm for the off-line grating. To adjust the gratings so that the on-line one coincided with the 946-nm water vapor absorption line and the other called the off-line did not coincide with any line, two aluminum yokes were constructed as shown in figure 16. Each fiber Bragg grating was epoxied to the ends of the aluminum yoke. The yokes consisted of an aluminum arc with a screw and an adjustment knob. By turning the adjustment knob, the screw pulled the arc apart and the fiber grating was stretched.

By stretching the fiber Bragg grating, the period of the grating increases and higher wavelengths are reflected according to equation (13). The adjustment knobs were turned until the on-line grating coincided with the 946.0003-nm water vapor line and the off-line grating was tuned to 945.9 nm. The final result is shown in figure 17.

16

Figure 17. Final reflection peaks of fiber Bragg grating and associated water vapor absorption lines.
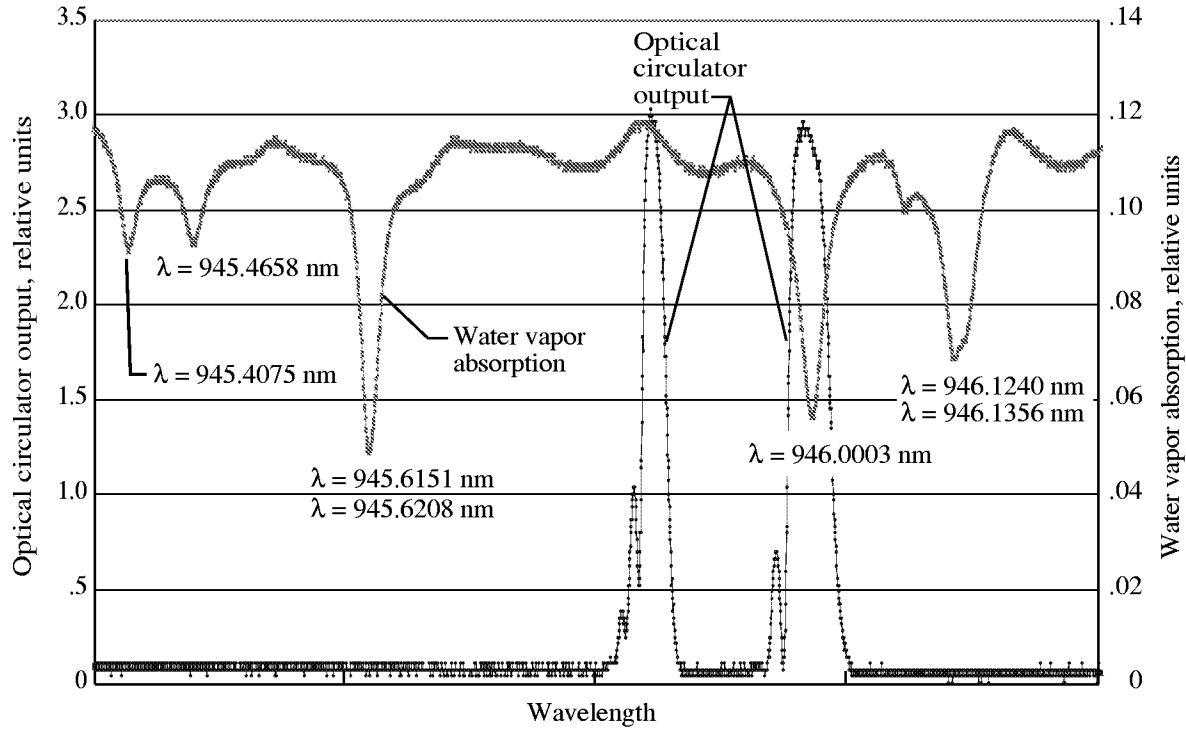
4.2. Bragg Grating Reflectivity and Bandwidth Measurement

The Bragg grating reflectivity and bandwidth were measured by using the setup of figure 11. The tunable diode laser was scanned through the Bragg grating reflection peaks while the photodiode at the end of the fiber grating recorded two dips in the laser output as the laser scanned through the gratings. Knowing the photodiode voltage that corresponded to no grating reflectivity and knowing that if the grating were 100 percent reflective, then zero voltage could be measured by the peak reflectivity as shown in figure 18. As shown in the figure, the on-line grating has a FWHM of 26 pm and a reflectivity of 93 percent, and the off-line grating has a FWHM of 32 pm and a reflectivity of 91 percent. These values should be compared with the theoretical value of equation (23) which gives a line width of 40 pm for a wavelength of 946 nm. The experimental value is a FWHM value, but the theoretical value is the distance between the first intensity minimum on both sides of the peak. This explains why the experimental values are slightly lower than the theoretical values.

4.3. Telescope Coupling Measurements

The setup shown in figure 14 was used to determine the spot size at the focal point of the telescope. The telescope has a diameter of 30 cm and a focal length of 60 cm. If parallel light is coming into the telescope, the minimum diffraction limited spot-size diameter at the focal point would be 8.3 μm. The typical minimum spot size was found to be 78×60 μm, which corresponds to an elliptical area of 4680 μm^2. This is a very large spot size compared with the area of the fiber to which it should be coupled. The diameter of the fiber is 9.3 μm, which corresponds to a mode field area of 67.9 μm^2. Comparing the area of the fiber core with the spot size area results in an efficiency of 1.4 percent. This should be compared with the measured coupling efficiency of the light at the telescope focal point compared with light emerging from the single-mode fiber. This efficiency was found to be 0.46 percent.
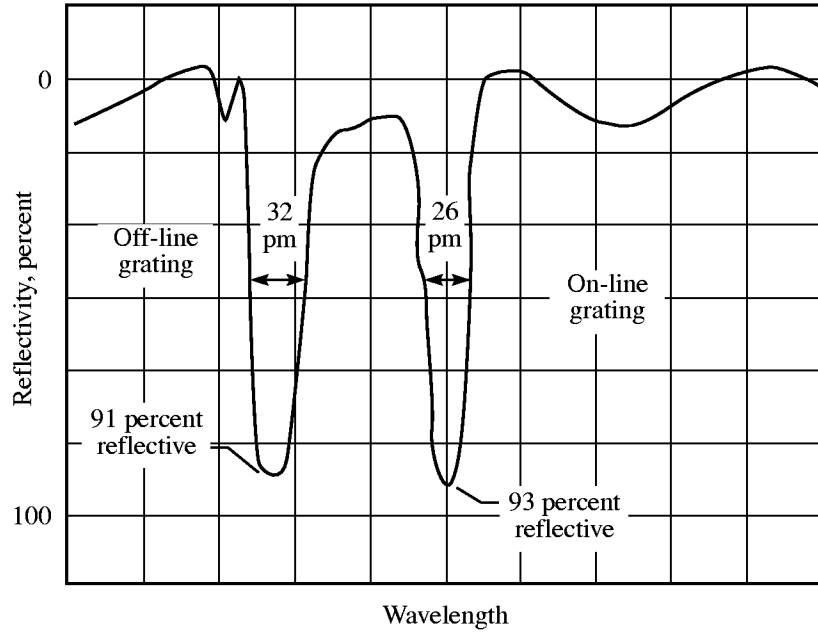
17

Figure 18. On- and off-line fiber Bragg grating for wavelength of 940 nm.

A multimode fiber was also tried in the experiment due to its larger diameter core. However it was found that a multimode fiber cannot be coupled to the circulator, the reflection peaks were smeared out; therefore, in this filter, a multimode fiber is not an option.

4.4. Receiver Efficiency Measurements

A setup like that of figure 11 was used to measure the efficiencies of this filter concept. The intensities at all the different steps in the receiver were measured with a power meter. The efficiencies are an average of three measurements and are shown in figure 19. To maximize the transmission in the circulator, the alignment is crucial and quite complicated. At port 1 and port 2, x, y, z, θ, and ϕ were adjusted carefully. It is necessary to iterate back and forth between the two ports to get the maximum output at port 2. The different efficiencies in figure 19 were measured step by step in the following way and they are summarized in table 1.

In measurement from path $0 \rightarrow 1$, light entered the telescope from the tunable diode laser. It was then reflected by the telescope into a single-mode fiber placed at the focal point of the telescope. The intensity before entering the telescope was measured compared with the intensity leaving the far end of the fiber. The efficiency was found to be 0.42 percent.

Measurement from path $1 \rightarrow 2$ was made by comparing the measured intensity leaving the single-mode fiber before entering the circulator at port 1 with the measured intensity leaving the circulator at port 2, with the fiber port removed. The efficiency was 83 percent which is a very good value compared with the optimal value of 85 percent found by the manufacturer.

Measurement from path $2 \rightarrow 4$ was made by comparing the intensity leaving the far end of the fiber Bragg grating at a wavelength that was not reflected by the grating with the measured intensity leaving the circulator at port 2 with the fiber port removed. The efficiency was found to be 52 percent.
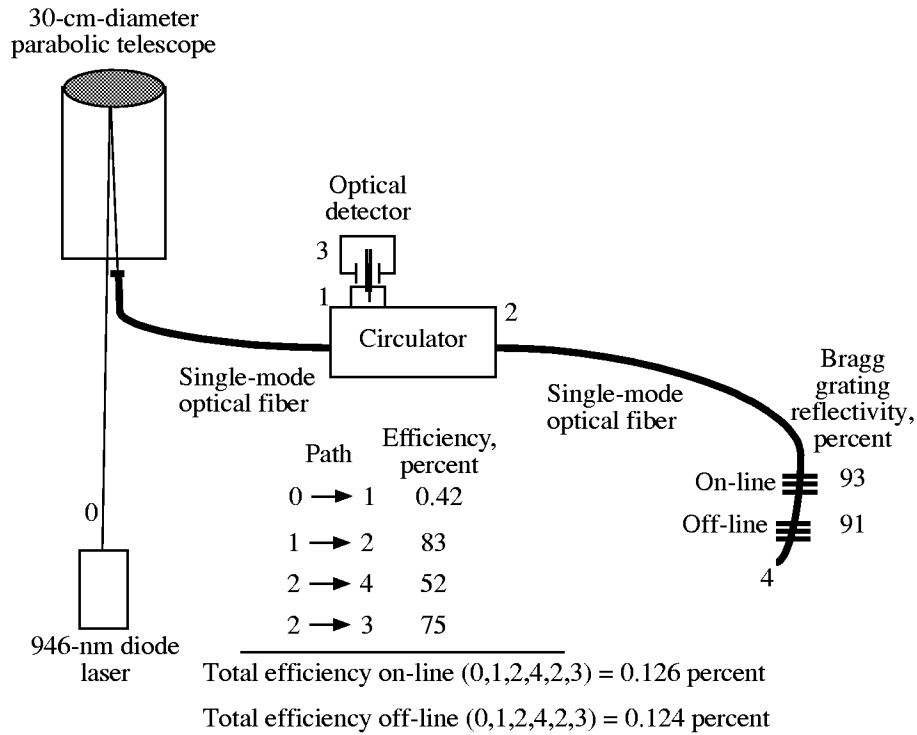
18

30-cm-diameter
parabolic telescope

Optical
detector

3

1

Circulator

2

Single-mode
optical fiber

Single-mode
optical fiber

Bragg
grating
reflectivity,
percent

Path	Efficiency, percent
0 → 1	0.42
1 → 2	83
2 → 4	52
2 → 3	75

On-line 93

Off-line 91

0

4

946-nm diode
laser

Total efficiency on-line (0,1,2,4,2,3) = 0.126 percent

Total efficiency off-line (0,1,2,4,2,3) = 0.124 percent

Figure 19. Receiver efficiency step by step.

Table 1. Explanations for Figure 19

Path	Input measurement	Output measurement	Efficiency, percent	Comments
0 → 1	Laser input at 946 nm to telescope	Output from single-mode fiber before circulator port 1	0.42	Poor coupling of telescope spot size to single-mode fiber
1 → 2	Output of fiber before entering fiber port 1	Output of circulator at port 2, with port removed	83	Manufacturer gives optimal transmission of 85 percent (without removing fiber port)
2 → 4	Output of port 2 of circulator with port removed	Output from end of fiber Bragg grating, laser tuned off grating	52	Poor coupling at fiber port 2
2 → 3	Light sent into far end of fiber Bragg grating; input measured while fiber disconnected from port 2	Output at port 3	75	Manufacturer gives optimal transmission of 81 percent

Measurement from path 2 → 3 was made by using a separate fiber port to enter light at the far end of the fiber Bragg grating. The intensity leaving the fiber Bragg grating before entering at port 2 was compared with the intensity leaving the circulator at port 3 at a wavelength that was not reflected by the Bragg grating. The efficiency was found to be 75 percent, which is a very good value compared with the optimal value of 81 percent found by the manufacturer.

19

As can be seen, the greatest loss is the coupling between the telescope and the fiber. The efficiency of the filter without the telescope is 30.1 percent for the on-line and 29.5 percent for the off-line. These numbers should be compared with the efficiency of a commercial 300-pm dielectric interference filter which is about 50 percent. Bear in mind that the bandwidth of fiber Bragg grating is much smaller.

5. Discussion of Results

When using optical filters in lidar receiver systems, the two major issues of primary concern are the optical transmission and bandwidth. Ideally the filter would have 100 percent transmission and a transmission bandwidth corresponding to the optical source bandwidth. The fiber Bragg grating described in this research effort approximates this ideal filter by having a reasonable optical transmission and very narrow bandwidth. It also has the ability to be easily tuned.

To demonstrate and characterize the performance of the ultra narrow bandwidth fiber Bragg grating filter, an experimental program was undertaken to measure the bandwidth, grating reflectivity, and the overall efficiency of the filter. A reflectivity of 91 percent and a bandwidth of 32 pm were measured for the off-line grating (945.9 nm) and a reflectivity of 93 percent and a bandwidth of 26 pm for the on-line grating (946.0003 nm). The length of the gratings was 2.5 cm. The reflectivity can be made almost 100 percent by making the grating somewhat longer, for example 3 cm; this would make the bandwidth slightly smaller. Another way of making the reflectivity higher is to choose a higher Δn, that is, a higher periodic change in the refractive index of the grating; this would be at the cost of a slightly broader bandwidth.

The efficiency of the filter is about 30 percent after the telescope light has entered the single-mode fiber, which is good compared with commercial filters, which have an efficiency of approximately 50 percent. Figure 19 and table 1 show that the transmission when passing through the circulator, port 1 to port 2 and port 2 to port 3, is comparable with the transmission indicated by the circulator manufacturer. The coupling from port 2 and into the fiber Bragg grating could be improved with better alignment of the circulator; however, aligning the circulator is not trivial. The ports tend to get stuck and the alignment could be lost or could deteriorate with time or with changes in room temperature. There may be a better way of constructing the filter without using a circulator. The largest loss in the filter is when light is coupled from the telescope into the fiber. Theoretically the spot-size diameter should be limited by diffraction to 8.3 μm, which should couple well to a fiber with a core diameter of 9.3 μm. However a typical spot size measured was 78 × 60 μm, which corresponds to an area of 4700 μm^2. If this area is compared with the core area of the fiber of 67.9 μm^2, only 1.4 percent of the light is coupled to the fiber. Experimentally an efficiency of 0.46 percent was measured. The difference could be explained by poor alignment of the fiber and the telescope. To get the minimum spot size at the focal point of the telescope, parallel light should enter the telescope. More research needs to be done on the coupling of the telescope light into the single-mode fiber. A larger fiber with a diameter of 68 μm was used, but it allowed multimode transmission and the circulator did not work correctly. The reflection peaks are smeared out, and one is not separated from the other.

An important improvement in the signal-to-noise ratio can also be made with a fiber Bragg grating filter. Because the bandwidth is much smaller, less of the atmospheric background radiation and broadband light reflected by Earth is detected. An improvement of the signal-to-noise ratio by almost 50 percent can be made as shown in figure 5.

Figure 8 shows the reflectivity as a function of Bragg grating length for different values of refraction index change Δn. With Δn of 5 × 10^{-5} and a grating of 2.5 cm as was used in this experiment, the reflectivity should theoretically be 100 percent. Experimentally a reflectivity of 91 percent was

measured for the off-line grating and 93 percent for the on-line grating. The experimentally measured values are shown as stars in the figure.

Figure 9 shows the bandwidth as a function of Bragg grating length for different values of refractive index change Δn. A 2.5-cm-long grating with a refractive index change Δn of 5×10^{-5}, like the grating used in the experiment, should theoretically have a bandwidth of 40 pm. A bandwidth of 32 pm was experimentally measured for the off-line grating and a bandwidth of 26 pm for the on-line grating. The bandwidth calculated theoretically is the width between the first two minima on either side of the reflection peak. The experimental bandwidth however is the FWHM, which explains why the experimental values are smaller than the theoretical one.

Another advantage of this filter compared with commercial filters is that the on- and off-line wavelengths can be tuned independently, which is not possible with the commercial filters. Rapid tuning could be accomplished by attaching the grating to a piezoelectric crystal. Commercial filters are too broad, covering both on- and off-line water vapor absorption lines. A fiber Bragg grating filter is compact and has low mass. It is therefore easy to transport and it would be possible to place it on an Earth-orbiting satellite.

6. Concluding Remarks

Fiber Bragg gratings have the potential for providing very narrow bandwidth optical filters for water vapor DIAL (differential absorption lidar) aircraft, space lidar receiver systems, and other filter applications. The filter bandwidth can be made as narrow as the water vapor absorption line, and separate filters can be used for on- and off-line DIAL atmospheric measurements.

An ultra narrow bandwidth filter using fiber Bragg gratings was found to have a bandwidth of 32 pm and a high reflectivity of about 91 percent for the off-line (945.9 nm) and a bandwidth of 26 pm and a reflectivity of 93 percent for the on-line (946.0003 nm). The measured values agree well with theory. Theoretically the reflectivity is 100 percent and the bandwidth 40 pm. However the bandwidth obtained theoretically is the bandwidth between the first two minima and the bandwidth measured experimentally is the FWHM (full width, half maximum). This difference explains why the experimental bandwidth is actually smaller than the theoretical bandwidth.

The on- and the off-line Bragg filters can be tuned separately, unlike commercial dielectric filters. The Bragg filters can be tuned easily by temperature or pressure. In the present research effort, the gratings were wavelength tuned by stretching them with an aluminum yoke.

Overall filter efficiency of 30 percent was achieved after light was coupled from the telescope into the fiber as compared with 50 percent for commercial filters. However more research needs to be done on the coupling from the telescope into the fiber.

An ultra narrowband fiber Bragg grating filter is a very promising way of measuring the water vapor content in the atmosphere from an Earth-orbiting DIAL satellite. With such a system, the understanding of pollution and the prediction of weather and hurricanes would improve.

Appendix

Description of Faraday Rotator and Half-Wave Plate

A1. Faraday Rotator

The Faraday effect is also called the magneto-optic effect. When linear polarized light propagates through a material medium such as glass and a strong external magnetic field is applied to the glass, the plane of polarization of the light will rotate an angle β (in minutes of arc) given by

$$\beta = VBd \qquad\qquad (A1)$$

where

B static magnetic flux, gauss

d   length of medium, cm

V factor of proportionality known as Verdet constant, min of arc/gauss/cm

The Verdet constant for a particular medium varies with frequency and temperature. A positive Verdet constant corresponds to a material in which the Faraday effect causes a counterclockwise (CCW) rotation when looking at the light source, and the light travels parallel to the applied B field. If the light propagates antiparallel to the B field, it is rotated clockwise (CW) as shown in figure A1. A Faraday rotator is used when a rotation of the polarization of the beam is needed in the same absolute direction, regardless of the direction of propagation of the beam along its axis. This effect does not occur in the case of natural optical activity. By reflecting a beam back and forth through a Faraday rotator the effect can be amplified (ref. 9).

The circulator in our experiment used a Faraday rotator to undo the effect of the half-wave plate when traveling from port 1 to port 2. When traveling from port 2 to port 3, the Faraday rotator and the half-wave plate together changed the o-wave into the e-wave and vice versa by rotating the polarization of each beam 90° so that they were reflected by the mirrors and exit at port 3.

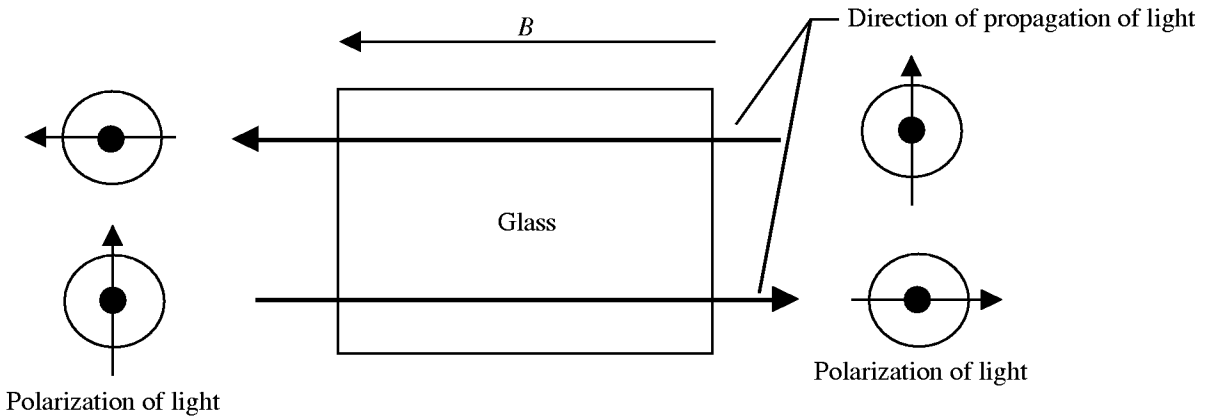Figure A1. Faraday effect with V > 0.

A2. Half-Wave Plate

A half-wave plate is made of a birefringent material, which means that the material has two different indices of refraction depending on the polarization of light: one for light polarized parallel to the optic axis of the material and one for light polarized perpendicular to the optic axis. The two polarization states travel at different velocities through the crystal, with the effect that a relative phase shift is introduced. A half-wave plate introduces a relative phase difference of 180° between the two polarization states. Light polarized parallel to the optic axis propagates with a higher speed than light polarized perpendicularly. Thus, the axis parallel to the optic axis is called the fast axis, and the axis perpendicular is called the slow axis. The slow axis in our experiment is inclined 22.5° to the horizontal and the fast axis is perpendicular to the slow axis. The half-wave plate rotates the component of the beam that is polarized parallel to the slow axis by 180°, thus rotating the total polarization of the beam 45° as explained in figure A2. Figure A2(a) shows the incoming polarization and its two components parallel to the fast and the slow axis. Figure A2(b) shows the outgoing light, after the component parallel to the slow axis has been rotated 180°. Figure A2(c) shows the incoming and the outgoing light, where the total polarization rotation is 45°. (See ref. 9.)

The circulator in our experiment used a half-wave plate together with a Faraday rotator to rotate the polarization 90° when traveling from port 2 to port 3. This rotation is done to change the o-beam into the e-beam and vice versa so that they are reflected by the mirrors and leave the circulator at port 3. When traveling from port 1 to port 2, the 45° rotation made by the half-wave plate is undone by the −45° rotation made by the Faraday rotator.
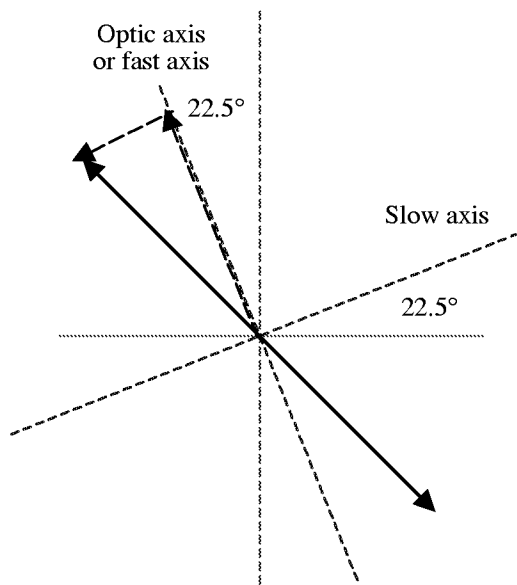
(a) Incoming polarization and two components of incoming light.
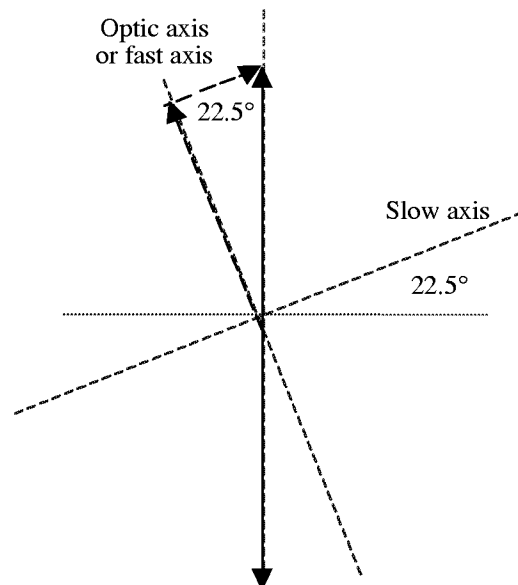
(b) Component parallel to slow axis rotated 180° with new polarization of light shown.
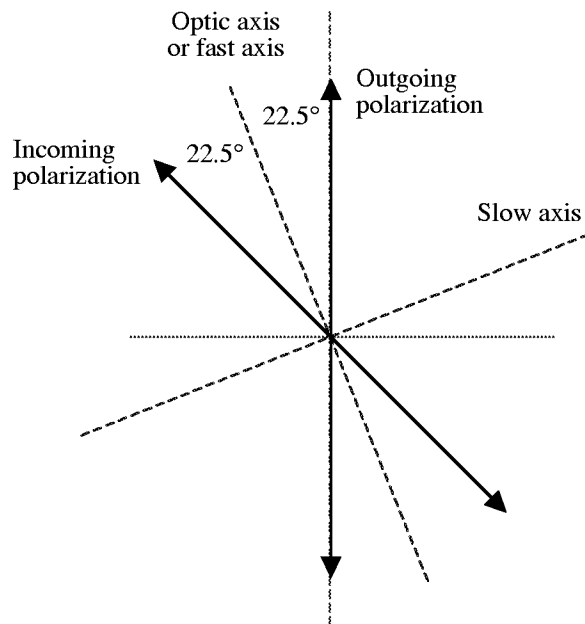
(c) Incoming and outgoing light with total polarization rotation of 45°.

Figure A2. Effect of half-wave plate.

References

1. Jursa, Adolph S., Sci. Ed.: *Handbook of Geophysics and the Space Environment*. Air Force Geophys. Lab., U.S. Air Force, 1985. (Available from DTIC as AD A167 000.)

2. Starr, D. O'C.; and Melfi, S. H., eds.: *The Role of Water Vapor in Climate: A Strategic Research Plan for the Proposed GEWEX Water Vapor Project (GVaP)*. NASA CP-3120, 1991.

3. EOS Science Plan (1999). NASA Goddard Space Flight Center, 1999. http://eospso.gsfc.nasa.gov/sci_plan/chapters.html Accessed September 27, 2001.

4. *Lidar Atmospheric Sensing Experiment (LASE): Measuring Water Vapor, Aerosols, and Clouds*. FS-2000-09-54-LaRC, NASA Langley Research Center, [2000].

5. Ismail, Syed; and Browell, Edward V.: Airborne and Spaceborne Lidar Measurements of Water Vapor Profiles: A Sensitivity Analysis. *Appl. Opt.*, vol. 28, no. 17, Sept. 1, 1989, pp. 3603–3615.

6. Measures, Raymond M.: *Laser Remote Sensing: Fundamentals and Applications*. John Wiley and Son, 1984.

7. Ghatak, Ajoy; and Thyagarajan, K.: *Introduction to Fiber Optics*. Cambridge Univ. Press, 1998.

8. Kashyap, Raman: *Fiber Bragg Gratings*. Academic Press, 1999.

9. Hecht, Eugene (with contributions by Alfred Zajac): *Optics*, Second Ed., Addison-Wesley Publ. Co., 1987.

REPORT DOCUMENTATION PAGE

Public reporting burden for this collection of information is estimated to average 1 hour per response, including the time for reviewing instructions, searching existing data sources, gathering and maintaining the data needed, and completing and reviewing the collection of information. Send comments regarding this burden estimate or any other aspect of this collection of information, including suggestions for reducing this burden, to Washington Headquarters Services, Directorate for Information Operations and Reports, 1215 Jefferson Davis Highway, Suite 1204, Arlington, VA 22202-4302, and to the Office of Management and Budget, Paperwork Reduction Project (0704-0188), Washington, DC 20503.

1. AGENCY USE ONLY *(Leave blank)*	2. REPORT DATE	3. REPORT TYPE AND DATES COVERED
	December 2001	Technical Memorandum

4. TITLE AND SUBTITLE
Ultra Narrowband Optical Filters for Water Vapor Differential Absorption Lidar (DIAL) Atmospheric Measurements

5. FUNDING NUMBERS
WU 622-63-13-70

6. AUTHOR(S)
Ingrid Stenholm and Russell J. DeYoung

7. PERFORMING ORGANIZATION NAME(S) AND ADDRESS(ES)

NASA Langley Research Center
Hampton, VA 23681-2199

8. PERFORMING ORGANIZATION REPORT NUMBER

L-18108

9. SPONSORING/MONITORING AGENCY NAME(S) AND ADDRESS(ES)

National Aeronautics and Space Administration
Washington, DC 20546-0001

10. SPONSORING/MONITORING AGENCY REPORT NUMBER

NASA/TM-2001-211261

11. SUPPLEMENTARY NOTES
Stenholm: Lund University, Lund, Sweden; DeYoung: Langley Research Center, Hampton, VA.

12a. DISTRIBUTION/AVAILABILITY STATEMENT

Unclassified–Unlimited
Subject Category 74   Distribution: Standard
Availability: NASA CASI (301) 621-0390

12b. DISTRIBUTION CODE

13. ABSTRACT *(Maximum 200 words)*
Differential absorption lidar (DIAL) systems are being deployed to make vertical profile measurements of atmospheric water vapor from ground and airborne platforms. One goal of this work is to improve the technology of such DIAL systems that they could be deployed on space-based platforms. Since background radiation reduces system performance, it is important to reduce it. One way to reduce it is to narrow the bandwidth of the optical receiver system. However, since the DIAL technique uses two or more wavelengths, in this case separated by 0.1 nm, a fixed-wavelength narrowband filter that would encompass both wavelengths would be broader than required for each line, approximately 0.02 nm. The approach employed in this project is to use a pair of tunable narrowband reflective fiber Bragg gratings. The Bragg gratings are germanium-doped silica core fiber that is exposed to ultraviolet radiation to produce index-of-refraction changes along the length of the fiber. The gratings can be tuned by stretching. The backscattered laser radiation is transmitted through an optical circulator to the gratings, reflected back to the optical circulator by one of the gratings, and then sent to a photodiode. The filter reflectivities were >90 percent, and the overall system efficiency was 30 percent.

14. SUBJECT TERMS
DIAL; Lidar; Water vapor; Bragg grating

15. NUMBER OF PAGES
34

16. PRICE CODE

17. SECURITY CLASSIFICATION OF REPORT	18. SECURITY CLASSIFICATION OF THIS PAGE	19. SECURITY CLASSIFICATION OF ABSTRACT	20. LIMITATION OF ABSTRACT
Unclassified	Unclassified	Unclassified	UL